Author/s:
Rahim, MA;Björnmalm, M;Bertleff-Zieschang, N;Ju, Y;Mettu, S;Leeming, MG;Caruso, F

Title:
Multiligand Metal-Phenolic Assembly from Green Tea Infusions

Date:
2018-03-07

Citation:
Rahim, M. A., Björnmalm, M., Bertleff-Zieschang, N., Ju, Y., Mettu, S., Leeming, M. G. & Caruso, F. (2018). Multiligand Metal-Phenolic Assembly from Green Tea Infusions. ACS Applied Materials and Interfaces, 10 (9), pp.7632-7639. https://doi.org/10.1021/acsami.7b09237.

Persistent Link:
https://hdl.handle.net/11343/191261

Multi-Ligand Metal–Phenolic Assembly from Green Tea Infusions

Md. Arifur Rahim,[1] Mattias Björnmalm,[1] Nadja Bertleff-Zieschang,[1] Yi Ju,[1] Srinivas Mettu,[2] Michael G. Leeming,[3,4] and Frank Caruso[1,*]

Affiliations

[1]ARC Centre of Excellence in Convergent Bio-Nano Science and Technology, and the Department of Chemical and Biomolecular Engineering, The University of Melbourne, Parkville, Victoria 3010, Australia

[2]Department of Chemical and Biomolecular Engineering, The University of Melbourne, Parkville, Victoria 3010, Australia

[3]School of Chemistry, The University of Melbourne, Parkville, Victoria 3010, Australia

[4]Bio21 Institute of Molecular Science and Biotechnology, The University of Melbourne, Parkville, Victoria 3010, Australia

Keywords: catechins, rust, etching, chelates, self-assembly, metal-phenolic networks, capsules

Abstract

The synthesis of hybrid functional materials using the coordination-driven assembly of metal–phenolic networks (MPNs) is of interest in diverse areas of materials science. To date, MPN assembly has been explored as mono-ligand systems (i.e., containing a single type of phenolic ligand) where the phenolic components are primarily obtained from natural sources via extraction, isolation, and purification processes. Herein, we demonstrate the fabrication of MPNs from a readily available, crude phenolic source—green tea (GT) infusions. We employ our recently introduced rust-mediated continuous assembly strategy to prepare these GT MPN systems. The resulting hollow MPN capsules contain multiple phenolic ligands and have a shell thickness that can be controlled through the reaction time. These multi-ligand MPN systems have different properties compared to the analogous MPN systems reported previously. For example, the Young's modulus (as determined using colloidal-probe atomic force microscopy) of the GT MPN system presented herein is less than half that of MPN systems prepared using tannic acid and iron salt solutions, and the disassembly kinetics are faster (~50%) than other, comparable MPN systems under identical disassembly conditions. Additionally, the use of rust-mediated assembly enables formation of stable capsules under conditions where the conventional approach (i.e., using iron salt solutions) result in colloidally unstable dispersions. These differences highlight how the choice of phenolic ligand and its source, as well as the assembly protocol (e.g., using solution-based or solid-state iron sources), can be used to tune properties of MPNs. The strategy presented herein expands the toolbox of MPN assembly while also providing new insights into the nature and robustness of metal–phenolic interfacial assembly when using solution-based or solid-state metal sources.

Introduction

The assembly of metal–phenolic networks (MPNs) has recently been introduced as a versatile platform for preparing functional hybrid materials.[1-5] This assembly process exploits the coordination interactions between transition metals and phenolic compounds—bearing catechol and galloyl functional groups (e.g., tannic acid)—inducing interfacial-assembly and formation of MPN films.[2,6-8] The preparation of MPNs in the form of bulk materials (in contrast to thin films) via direct gelation of polyphenols, using similar coordination chemistry, has also recently been demonstrated.[9] Besides this coordination-driven assembly, phenolic compounds such as dopamine have also been shown capable of forming coatings (but via oxidative polymerization instead of through complexation).[10] The discovery of these types of systems originated from the chemistry of adhesive proteins in mussels.[10] The resulting polydopamine (PDA) materials have shown potential applications in diverse fields ranging from biomedicine to catalysis.[11-16] Despite the differences in molecular interactions, assembly conditions, and formation kinetics between MPN-based and PDA-based systems, both coatings have been established as facile and versatile surface-modification techniques.[4,16-17]

Recently, we introduced a continuous assembly strategy for MPN synthesis exploiting rusted iron objects (e.g., iron nails) as solid-state metal sources, instead of the metal salt solutions used in the conventional method.[18] Using this approach, the fundamental nature of MPN assembly can be modulated from discrete to continuous.[18] These MPN-based materials are being explored for applications in diverse fields, ranging from drug delivery to catalysis.[4,19-27] Moreover, the vast library of available natural phenolic compounds (e.g., from plants, fruits, vegetables, grains, and many microorganisms)[28-33] provides an immense source of inspiration and possible routes for exploring different metal–phenolic systems, utilizing various coordination chemistries and displaying diverse functionalities.

A common and rich source of phenolic compounds is green tea (GT).[34-36] The beneficial health effects associated with GT consumption include its anti-oxidative, anti-inflammatory, and anti-carcinogenic properties—largely attributed to the phenolic contents known as green tea catechins (GTCs).[34,36-39] Besides these biofunctional properties, GT has also been of interest in materials science, for example for noble metal nanoparticle synthesis and surface modification, where the chemical properties of GTCs (e.g., coordination/chelation and reducing capabilities) have been exploited.[40-43] We hypothesized that GT infusions (based on the water solubility of GTCs and their reported concentration range in these type of infusions)[35,44-45] could serve as a direct and readily available phenolic source for fabricating MPNs incorporating multiple catechin ligands in a single system.

Herein, we explore GT infusions as alternative phenolic sources for MPN assembly, and combine this concept with the rust-mediated continuous assembly approach[18] to demonstrate the synthesis of multi-ligand MPN systems. The MPN systems presented herein: (i) use phenolic and metallic components from common sources, thus demonstrating that extraction, separation, and purification processes of phenolic and metallic components are not prerequisites for MPN assembly, with potential implications for widespread and large-scale synthesis and application of MPNs; (ii) explore key differences between conventional and continuous MPN assembly approaches, including the ability to maintain colloidal stability by leveraging a double dynamic assembly process (i.e., etching and self-assembly); and (iii) demonstrate that multiple phenolic ligands can be simultaneously incorporated during MPN assembly, thus highlighting the versatility of the underlying coordination chemistry while providing a new strategy for tailoring properties and functionality of MPN-based materials.

Experimental Section

Materials. Commercial green tea bags from multiple brands (Twinings, Dilmah, and Tetley) were purchased from a local market. Commercial bright steel nails (Paslode, diameter × height: 2.8 mm × 50 mm, product number N906600) were purchased from Bunnings, Australia. Iron(III) chloride hexahydrate ($FeCl_3 \cdot 6H_2O$), epigallocatechin gallate (EGCG), epicatechin gallate (ECG), and poly(ethylenimine) (PEI, M_W = 25 kDa) were purchased from Sigma-Aldrich and used as received. Poly(methyl methacrylate) (PMMA) microparticles (D = 3.69 ± 0.08 μm) were purchased from Microparticles GmbH. *N*-methyl pyrollidone (NMP) and acetone were purchased from ChemSupply. High-performance liquid chromatography (HPLC)-grade acetonitrile and formic acid were obtained from Merck and BDH, respectively. High-purity (Milli-Q) water with a resistivity of 18.2 MΩ·cm was obtained from an inline Millipore RiOs/Origin water purification system.

Characterization. Differential interference contrast (DIC) microscopy images were taken with an inverted Olympus IX71 microscope. Ultraviolet–visible (UV–vis) absorption spectra were collected on a Varian Cary 4000 UV–vis spectrophotometer. Atomic force microscopy (AFM) experiments were carried out with a JPK NanoWizard II BioAFM. Typical scans were performed in tapping mode with MikroMasch silicon cantilevers (NSC/CSC). The film thickness and roughness of the air-dried capsules were analyzed (at least 20 different capsules for each sample) using JPK SPM image processing software (version V.3.3.32). Transmission electron microscopy (TEM) images and energy dispersive X-ray spectroscopy (EDX) profiles were acquired using a FEI Tecnai TF20 instrument with an operation voltage of 200 kV. In AFM and TEM/EDX experiments, the capsule suspensions (2–10 μL) were allowed to air-dry on glass slides (Piranha cleaned) and formvar-carbon coated copper grids, respectively.

Liquid chromatography-mass spectrometry (LC-MS) experiments were carried out using an Agilent 6520 quadrupole time-of-flight (Q-TOF) mass spectrometer coupled to an Agilent 1200 series liquid chromatography system (Palo Alto, CA). For each analysis, 5 µL of the samples, i.e., GT infusions, EGCG (2 mg mL^{-1} in H_2O), ECG (1 mg mL^{-1} in H_2O), and disassembled capsules (see below for conditions), were injected and compounds were separated by an Agilent ZORBAX Eclipse XDB C_{18} reversed phase column (150 × 4.6 mm, 5 µm) over a 50 min solvent gradient using 100% Milli-Q water as mobile phase A and 70% acetonitrile in 0.1% formic acid (v/v) as mobile phase B (flow rate of 0.3 mL min^{-1}). The gradient timetable was as follows [time (min), %B]: [0,0], [1,0], [41,100], [44,100], [45,0], [50,0]. The column was maintained at 25 ± 0.8°C throughout all analytical runs and samples were held in an autosampler chamber at 4°C prior to analysis. Compounds eluting from the column were transferred to the gas phase via electrospray ionization (ESI). Analyses were conducted in the negative ion mode and spectra were acquired over the range *m/z* 50–1000. ESI parameters were as follows: drying gas flow rate and temperature = 12 L min^{-1}, 300ºC; capillary voltage = 3.5 kV; skimmer voltage = 65 V; fragmentor voltage = 75 V; Octapole RF_{Vp-p} = 750 V.

Rusting of Iron Nails. Commercial iron nails were rusted according to our previous report.[18] Briefly, iron nails were degreased first by wiping with acetone-wet tissue (Kimwipe) and then sonicated in acetone for 10 min. The degreased nails were then thoroughly washed with Milli-Q water and air-dried. Next, 51 mL of 10% HCl was taken in a 250 mL glass beaker. The washed nails were placed from top of the beaker with a gap of 3.8 cm from the top surface of the HCl solution and the beaker was kept in a fume hood. After 20 h, adherent rust layers were observed to have formed on each nail surface and the rusted nails were removed from the beaker. After incubation in Milli-Q water for 10 min, the rusted nails were thoroughly washed with Milli-Q water and air-dried. The dried rusted nails were stored under vacuum before use.

GT/R-Fe^{III} Film Formation on Particulate Substrates. GT infusions were prepared by submerging two tea bags in hot (~90 °C) tap water (200 mL, 3 min; note that tap water and not high-purity Milli-Q water was used for this step), cooled down to room temperature (~22 °C), and filtered through a membrane filter (0.22 μm pore size). Filtered GT infusions (10 mL) were taken into 15 mL tubes and the pH adjusted to 5 by addition of HCl solution (1 M, 20 μL). Subsequently, PMMA particles (500 μL, 10% w/v, aqueous suspension) and a rusted nail (see "Rusting of Iron Nails" above) were then added. The tubes were kept under constant shaking (using a rotating wheel, ~40 rpm) during the MPN coating process. Aliquots of 300 μL of GT/R-Fe^{III} (R-Fe^{III} denotes iron(III) ions sourced from rust) coated PMMA particles were taken at different time points (for standard characterization, particles were taken out after 40 min) and unreacted supernatant was discarded after centrifugation (1900 *g*, 1 min), followed by four washing cycles[5]: centrifugation at 1900 *g* for 1 min, supernatant discarded, and particle pellet resuspended in 500 μL of Milli-Q water. Dissolution of PMMA template particles was achieved through five washing cycles: as above but using 500 μL of NMP/acetone (1:1 v/v) instead of Milli-Q, and performing the centrifugation at 2200 *g*. In the first three dissolution steps the coated particles were incubated for 30 min each to facilitate complete removal of PMMA. The obtained hollow capsules were washed twice (2200 *g*, 2 min) with Milli-Q water and finally resuspended in 100 μL of Milli-Q water for characterization. For the time-dependent thickness increase studies of GT/R-Fe^{III} films, aliquots were taken out at 20, 40, 60, and 90 min and processed as above to obtain hollow capsules at each time point.

GT/Fe^{III} Film Formation on Particulate Substrates by Conventional Method. GT infusions were prepared as above and the pH was adjusted to 5 using HCl solution (1 M, 20 μL). GT infusions (400 μL) were added to PMMA particles (50 μL, 10% w/v, aqueous suspension) and mixed by repeated pipetting ("up and down"). $FeCl_3 \cdot 6H_2O$ solution (30 mM, 100 μL) was then added and the mixture quickly vortexed for 3−4 s. Subsequently, the mixture

pH was raised by addition of NaOH solution (1 M, 7 μL) followed by vortexing for 1 min. After coating, the particles were processed in identical manner as above to obtain hollow capsules. The coating process was also tested with 2- and 3-fold dilutions (v/v, in water) of the starting compounds.

Disassembly Experiments. GT/R-Fe^{III} capsule (~11 nm shell thickness) suspensions (~4×10^7 capsules mL^{-1}) were mixed with an equal volume of disassembly solution (KCl-HCl buffer, 100 mM, pH 2). Disassembly (in terms of film composition) was monitored for each system by UV–vis absorption spectroscopy by the decrease in the ligand to metal charge transfer (LMCT) band intensity with time.

Analyses of the Organic Fragments of Disassembled Capsules. 500 μL of concentrated GT/R-Fe^{III} capsule suspensions (~3×10^9 capsules mL^{-1}) was mixed with HCl (6 M, 1 mL) under vortexing and kept on a rotating tube mixer for 10 min. The mixture was then diluted with an equal volume of Milli-Q water and lyophilized to remove excess HCl. Lyophilized products were resuspended in 300 μL of acidified methanol (prepared by adding 10 μL of 0.1 M HCl to 1 mL of methanol), and filtered through a 0.8 μm membrane filter before analysis using LC-MS.

Mechanical Tests. Details of the AFM force measurements and colloidal probe preparation can be found elsewhere.[6,46] Briefly, the measurements were performed on a NanoWizard II (JPK) in Milli-Q water using colloidal probe cantilevers. To fabricate the modified cantilevers, tipless cantilevers (MLCT-O, Bruker AFM Probes) were used. A spherical glass bead (D = 28.2 μm, Polysciences) was attached to the cantilever using an epoxy resin (Selleys Araldite Super Strength, Selleys) via micromanipulation employing an AFM system and associated optics. The probe was then allowed to dry overnight. Glass slides and cantilevers were cleaned with isopropanol, water, and plasma treatment to remove adventitious contamination. The

modified cantilevers were first calibrated on a cleaned glass substrate to determine the inverse optical lever sensitivity (InvOLS), and the spring constant was determined to be 0.122 N m^{-1} using the thermal noise method. PEI-coated glass slides were used to immobilize the capsules prior to the measurements. Force-distance curves were obtained by optically positioning the probe over individual capsules (GT/R-Fe^{III} capsules with ~11 nm shell thickness) and an approach-retract cycle with a force load of 2.5 nN and a constant piezo velocity of 1 μm s^{-1} was initiated. Force spectra of at least 10 different capsules per system were collected and analyzed using JPK data processing software. A baseline was first subtracted from the noncontact z-range of the force-displacement data and a probe/surface contact point was assigned. After subtracting the effect of the cantilever bending, force-deformation (F-δ) data were obtained. The Young's modulus (E_Y) of the spherical capsules could be estimated using the Reissner model for thin-walled spherical shells. The E_Y of GT/R-Fe^{III} capsules (~11 nm shell thickness) was determined using the Reissner equation with a wall thickness (h) of 11 nm, a Poisson's ratio (ν) of 0.5, and an effective probe radius (R_{eff}) of 1.85 μm. Only the deformation data over the capsule shell thickness was used.

Results and Discussion

GT is a complex mixture of catechins, proteins, vitamins, and minerals.[47-48] The dominant GTCs present in GT are epigallocatechin gallate (EGCG), epicatechin gallate (ECG), epigallocatechin (EGC), and epicatechin (EC).[35,44-45] The structures of these GTCs are shown in Figure S1. Liquid chromatography-mass spectrometry (LC-MS) performed on the GT infusions used in this study detected a range of phenolic compounds, as summarized in Figure S2 and Table S1. Comparing extracted ion chromatogram peak areas between pure catechin standards (Figure S3) and GT infusions, the concentrations of EGCG and ECG in the infusion

were estimated to be ~1.8 and ~2.7 mM, respectively. These results are in agreement with previous reports.[49-52]

Figure 1 depicts the experimental process for MPN assembly adapted in this study. GT infusions were prepared by submerging tea bags (Figure 1a) in hot water, and then filtering the infusions after they had cooled down to room temperature (Figure 1c-e). To initiate MPN film formation, rusted nails (Figure 1b) were incubated in GT infusions containing particle templates (PMMA microparticles) as shown in Figure 1c-e. The GT/template dispersion turned increasingly blue-black over time (Figure 1f-h), which is typical during formation of coordination complexes involving iron(III) (Fe^{III}) and phenolic ligands containing catechol or galloyl function groups.[53-54] This suggests the coordinative etching of Fe^{III} ions from the rust layer by GTCs present in the GT infusion.[18] The GTC/Fe^{III} complexes thus generated were observed to self-assemble on the solid particle templates and subsequently formed stable MPN films and hollow capsules after template removal (see below).

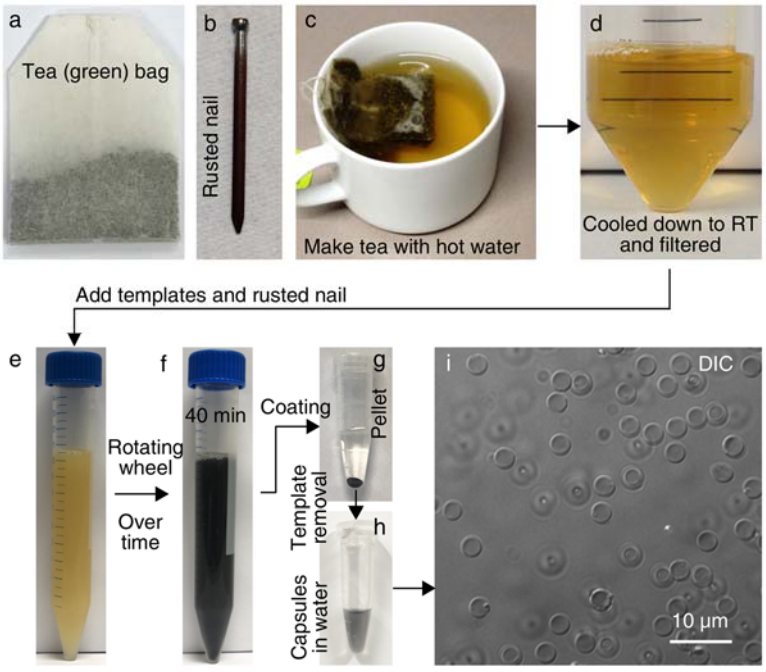

Figure 1. Photographs of a GT bag (**a**), rusted nail (**b**), initial GT infusion (**c**), and GT infusion after cooling and filtration (**d**). **e-h**, Photographs of the MPN assembly process in sequence.

Photographs showing the coating on PMMA templates (**g**) after washing and pelleting through centrifugation, and a concentrated dispersion of freestanding capsules (**h**) obtained after template removal and redispersion in water. **i**, DIC image of GT/R-Fe^{III} capsules.

The working duration for the continuous assembly of MPNs using GT infusions was examined by investigating the etching kinetics of rusted nails incubated in GT infusions (in the absence of template particles). The etching process was monitored by UV–vis absorption spectroscopy. As the etching progressed, the characteristic ligand-to-metal charge transfer (LMCT) band of GTCs/Fe^{III} complexes appeared at ~570 nm.[6,53,55] The LMCT band intensity was observed to increase as a function of time until a plateau was reached after around 3 h (Figure S4). Based on this saturation profile, we investigated the continuous assembly for film formation using GT infusions within this time range.

The films and capsules obtained after 40 min of immersion of the rusted nail in the GT/template dispersion were chosen as standard samples and extensively characterized. These MPN films are denoted as GT/R-Fe^{III}. The GT/R-Fe^{III} coatings can be observed through the dark coloration of coated template particles and free-standing capsules (after dissolution of the template particles) (Figure 1g,h). GT/R-Fe^{III} capsules were found to be stable, monodisperse and with negligible levels of aggregation as observed by differential interference contrast (DIC) microscopy (Figure 1i).

UV–vis absorption spectrum of the GT/R-Fe^{III} system (Figure 2a) showed the LMCT band at ~570 nm arising from a dominant bis-type (galloyl/Fe^{III}) coordination mode in the film structures.[6,18,55-56] UV–vis absorption spectrum for the GT infusion is also presented for comparison. The GT/R-Fe^{III} system was further investigated by atomic force microscopy (AFM). The dried GT/R-Fe^{III} capsules revealed surface morphologies with folds and creases, typical of collapsed capsules (Figure 2b).[5] From the AFM height profile analyses, the shell

thickness of the capsules was found to be ~11 nm (Figure S5) with a root-mean-square (rms) roughness value of ~1 nm. Transmission electron microscopy (TEM) images of the GT/R-Fe^{III} capsules showed similar morphologies as observed by AFM (Figure 2c). Energy dispersive X-ray (EDX) analyses performed on the dried capsules confirmed the presence of iron in the films (Figure 2d).

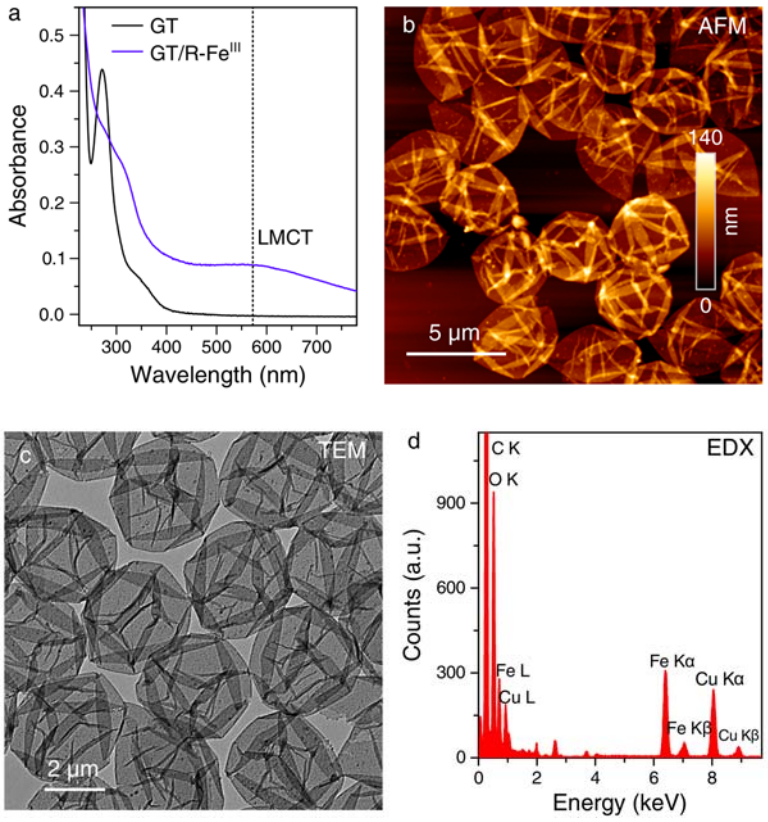

Figure 2. a, UV–vis absorption spectra of GT infusion (black solid line) and GT/R-Fe^{III} system (purple solid line) showing the LMCT band around ~570 nm (black dotted line). Surface morphologies of the GT/R-Fe^{III} capsules as observed by AFM (**b**) and TEM (**c**). **d**, EDX spectrum showing the presence of iron in the GT/R-Fe^{III} system. GT/R-Fe^{III} capsules were obtained after 40 min of immersion of the rusted nail in the GT/template dispersion.

The presence of multiple catechin ligands in the GT/R-Fe^{III} system was probed by LC-MS. The organic fragments of GT/R-Fe^{III} capsules after disassembly in concentrated HCl showed two dominant chromatographic peaks with retention times of ~23 and ~26 min, as

shown in Figure 3a. These peaks can be assigned to EGCG and ECG, respectively, as confirmed by comparing the retention times of pure EGCG and ECG (Figure S3). The mass spectra at the regions of peak maxima showed dominant ions at *m/z* 457.07 $[M-H]^-$ and 441.08 $[M-H]^-$, which can be attributed to EGCG (Figure 3b) and ECG (Figure 3c), respectively. Other minor peaks support these assignments, such as at *m/z* 493.05 (Figure 3b) and 477.05 (Figure 3c) observed in the spectra, which can be assigned to EGCG-chloride and ECG-chloride adducts, as evidenced by their chlorine isotope patterns.

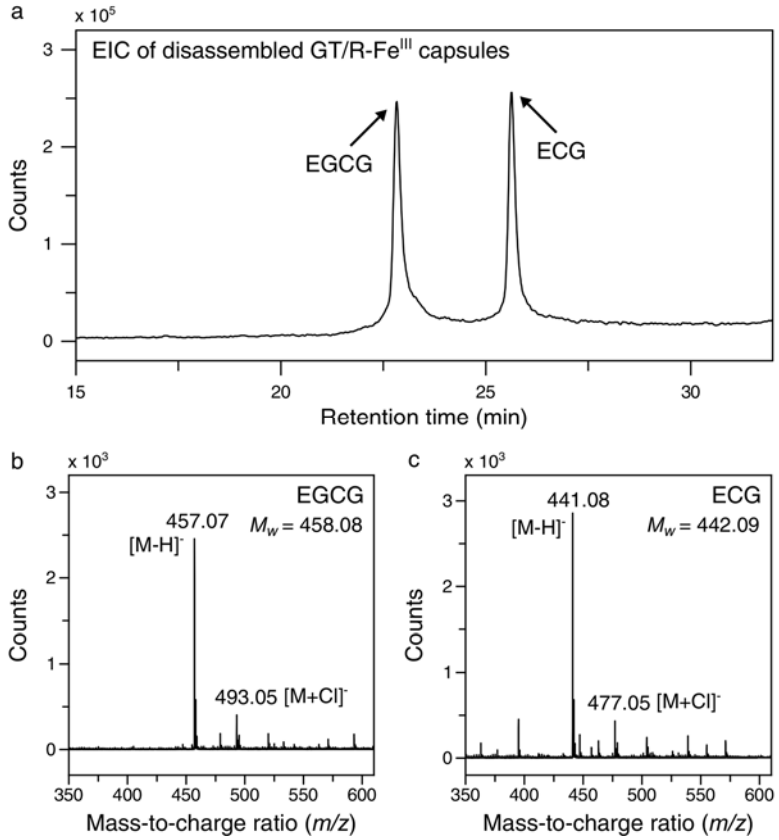

Figure 3. a, Combined extracted ion chromatograms (EIC) of EGCG (*m/z* 457.07) and ECG (*m/z* 441.08) derived from LC-MS analysis of disassembled GT/R-Fe^{III} capsules. **b-c**, Corresponding MS analyses of the detected compounds.

A salient feature of the continuous assembly approach is that it enables film thickness of the MPN systems to be controlled as a function of reaction time.[18] To investigate this

behavior for the GT/R-Fe^{III} system, samples were taken out at different time points (i.e., at 5, 10, 20, 40, 60, and 90 min) from the dispersion during the coating procedure, and the resulting GT/R-Fe^{III} capsules were analyzed. Samples taken after 5 and 10 min did not form stable capsules after template removal (in agreement with a previous report[18]), and were therefore not analyzed further. The film thicknesses of these capsules were examined by AFM and it was observed that the shell thickness of GT/R-Fe^{III} capsules increased in a time dependent manner (Figures 4 and S6), as expected. From AFM height profile analyses, the film thicknesses of GT/R-Fe^{III} capsules obtained at 20, 40, 60, and 90 min were found to be ~7, ~11, ~15, and ~22 nm, respectively (Figure 4c). This implies a growth rate of approximately 0.2–0.3 nm min^{-1}. The roughness (rms) values among these GT/R-Fe^{III} capsules with different thicknesses were around 1 to 2 nm. Moreover, the LMCT band (at ~570 nm) of the capsules with increasing thicknesses was observed to intensify over time (Figure 4d), which is in agreement with the AFM analyses above.

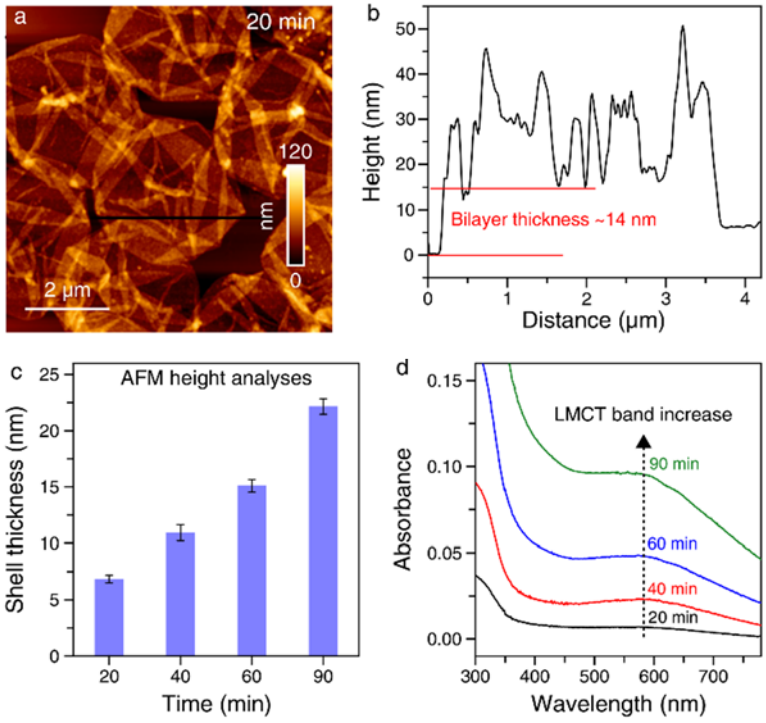

Figure 4. a-b, AFM topographic image and the corresponding height profile of GT/R-Fe^{III} capsules obtained after 20 min. **c**, AFM height analyses of GT/R-Fe^{III} capsules obtained at different time points showing increasing shell thickness. **d**, UV–vis absorption spectra of GT/R-Fe^{III} system at different time points showing the increase in LMCT band intensity.

GT infusions prepared from several different brands of commercial GT bags were also tested for MPN assembly. In each case, MPN film formation was successful, as presented by the UV–vis absorption spectrum and DIC images in Figures 5 (a, b) and S7. No differences in the quality of capsules prepared using all three brands of tea tested were observed.

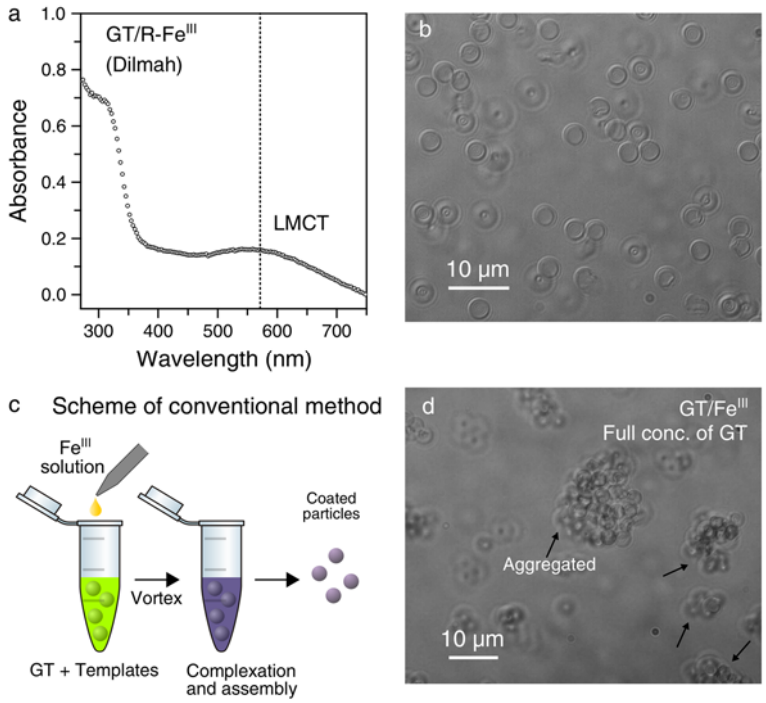

Figure 5. a-b, UV–vis absorption spectrum and DIC image of GT/R-Fe^{III} capsules prepared by another commercial brand of green tea. **c**, Scheme of the conventional method. **d**, DIC image showing the quality of GT/Fe^{III} capsules prepared using the conventional method (i.e., using Fe^{III} solution instead of rust as iron source) with a GT infusion as the phenolic source.

Using the conventional method (using Fe^{III} solutions instead of solid-state reactants) to obtain GT/Fe^{III} capsules was also attempted (Figure 5c). However, as soon as Fe^{III} solutions

were added to GT/template dispersions, the dispersions were observed to lose their colloidal stability and the template particles aggregated. This occurred when using undiluted, or 2-fold and 3-fold dilutions of pristine GT infusions. Moreover, in the washing steps, other forms of precipitates were found along with the template pellet. As a result, the final capsules obtained were observed to be aggregated and deformed, as seen in the DIC images (Figures 5d and S8). The colloidal instability, precipitate formation, and deformation of the capsules may be caused by a combination of the rise of ionic strength of the system upon addition of the Fe^{III} solution and the nonspecific interactions of Fe^{III} ions with other organic components present in the GT infusions (rather than the catechins). In contrast, in the continuous assembly method, Fe^{III} ions come to the solution as coordination complexes via specific etching of rust by GTCs present in GT infusion, thus avoiding the addition of salt species (which can change the ionic strength of the solution) and the induction of nonspecific interactions between Fe^{III} ions with organic compounds of the system. Thus, the capsule systems obtained through continuous assembly (i.e., GT/R-Fe^{III} capsules) are monodisperse, colloidally stable, and without any visible precipitates. This highlights a key difference between using conventional (solution-based) assembly[1] compared with continuous (solid-state reactant-based) assembly[18] for MPN film synthesis, which can be leveraged to improve processing properties and resulting film quality when working with different types of source materials, such as crude phenolic extracts.

We also investigated disassembly and mechanical properties of the standard GT/R-Fe^{III} capsule system with a shell thickness of ~11 nm (as shown in Figures 1 and 2). Disassembly profiles (in terms of film composition) of GT/R-Fe^{III} capsules incubated in buffer solutions of pH 2 were monitored by following the decrease in intensity of the LMCT band as a function of time. GT/R-Fe^{III} capsules were observed to be completely disassembled within 15 min (Figure 6a). Further analysis on the disassembly kinetics (Figure 6b) suggested that over 50% and 70% of capsules had disassembled after 2 and 6 min, respectively. This can be compared

to our previously reported GA/R-Fe^{III} system (where 'GA' denotes gallic acid) with a shell thickness of ~10 nm, which showed 50% disassembly at 3 min at identical disassembly conditions.[18]

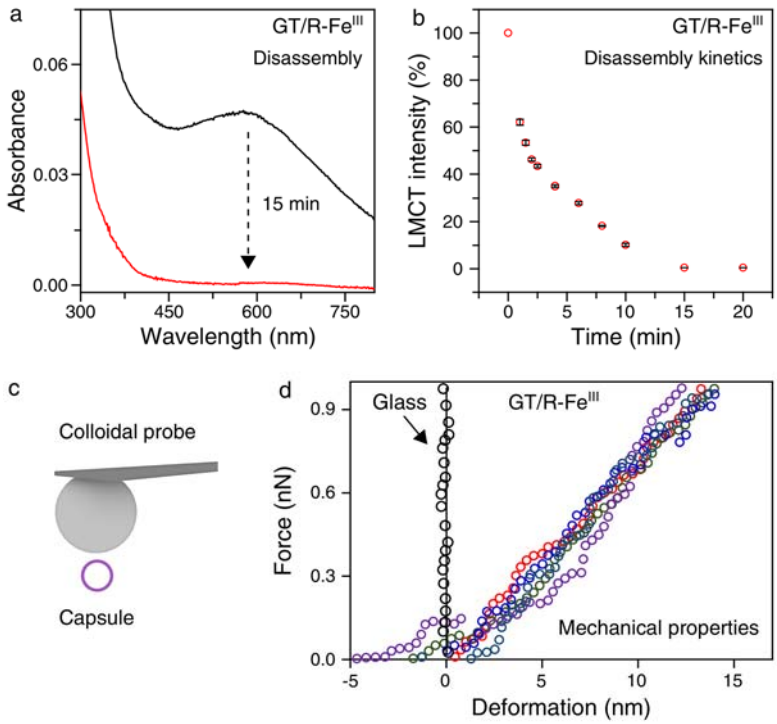

Figure 6. a, UV–vis absorption spectrum showing the LMCT band of the standard GT/R-Fe^{III} capsules before and after completion of the disassembly. **b**, The corresponding disassembly kinetics. **c**, Schematic presentation of an AFM colloidal probe used to investigate the mechanical properties of the GT/R-Fe^{III} capsules. **d**, Representative force-deformation curves for the small deformation regime of the GT/R-Fe^{III} capsules of ~11 nm shell thickness. A force-deformation curve for the glass substrate (black circles) is also shown for comparison.

Finally, we investigated mechanical properties of GT/R-Fe^{III} capsules using colloidal-probe AFM force measurements (Figure 6c). Representative force-deformation curves are shown in Figure 6d. By analyzing the slope of the curves, the stiffnesses of GT/R-Fe^{III} capsule was determined to be 76 ± 12 mN m^{-1} and the corresponding Young's modulus (E_Y) was estimated to be 433 ± 70 MPa. This can be compared to the reported E_Y of 334 ± 63 MPa for

GA/R-Fe^{III} capsules of ~10 nm thickness.[18] The deformation of capsules shown in Figure 6d is the measured deformation by AFM. However, it has recently been shown that the measured deformation from AFM is the sum of the deformations at the top and the bottom of the capsule.[57] Traditionally, AFM deformation without any modification has been used for calculating the mechanical properties of capsules.[1,6] However, in order to achieve more accurate estimates of mechanical properties, correction factors have been derived as a function of shell thickness, radii of AFM probe and capsule in order to convert the measured AFM deformation to effective capsule deformation.[57] The AFM probe used in our experiment is large (radius 14.1 μm) in comparison to the particle templates (radius 1.85 μm), and the shell thickness (11 nm) is small in comparison the capsule size (particle templates were 3.69 μm in diameter). Thus, Reissner's formula with a correction factor of 0.5 should be used to more precisely calculate the mechanical properties of the capsules under these conditions.[57] As a result, the more precise capsule shell stiffness (K_S) and Young's modulus (E_Y) are twice the values calculated without the use of a correction factor. The values of stiffness and modulus (after application of the correction factor) are 152 ± 24 mN m^{-1} and 866 ± 140 MPa, respectively.

Other previously reported MPN systems were found to be stiffer and exhibit different disassembly kinetics than those of the system presented here. For example, the Young's modulus reported here for GT/R-Fe^{III} capsules (433 ± 70 MPa) can be compared to what has been previously reported for tannic acid/Fe^{III} capsules (1000 ± 200 MPa),[1] pyrocatechol/Fe^{III} capsules (870 ± 240 MPa),[6] and GA/Fe^{III} capsules (620 ± 200 MPa).[6] When comparing disassembly kinetics, over 50% disassembly occurred after 2 min for the system presented here (GT/R-Fe^{III}), while for GA/R-Fe^{III} (mentioned above) and GA/Fe^{III} 50% disassembly occurred after 3 min and 4 min, respectively, under the same disassembly conditions.[18] Overall, these differences in properties in various MPN systems indicate that the assembly conditions,

molecular structures of the phenolic ligands, and modes of metal–phenolic coordination interactions can considerably impact the resulting networks and film properties. This may provide insights into the structure-function relationship of MPN systems and aid in the design of new system with properties tailored to specific application.

Conclusions

In summary, we have described the assembly of multi-ligand MPN systems where both phenolic and metallic components were sourced from daily life (i.e., green tea and rust). To the best of our knowledge, this is the first exploration of utilizing crude phenolic extracts (such as green tea infusions) for MPN assembly. The combination of green tea infusions and rust produced high quality colloidal coatings with multiple catechin ligands in a single MPN system. Key physicochemical properties of this MPN system—including assembly and disassembly kinetics, composition, morphology, and mechanical properties—were investigated. Comparisons (of using green tea infusions) between continuous (rust-mediated) and conventional (using solution-based iron sources) MPN assembly revealed striking differences: colloidal stability was lost (i.e., substantial particle aggregation occurred) for coatings prepared using the conventional assembly approach, but not when using the continuous assembly approach. This highlights a new aspect of the double dynamic process enabled by using solid state-reactants (i.e., etching and self-assembly), by demonstrating successful MPN assembly under conditions where the conventional assembly approach results in colloidally unstable dispersions. The presented strategy thus complements the conventional assembly approach and expands our understanding of metal–phenolic assembly, as well as

increase their usefulness under demanding conditions, such as performing assembly using crude extracts in resource-limited settings.

Associated Content

Supporting Information. The Supporting Information is available free of charge on the ACS Publications website. Additional AFM analysis, chemical structures, LC-MS analysis, etching kinetics, UV–vis absorption spectroscopy, and DIC images.

Author Information

Corresponding Author. *E-mail: fcaruso@unimelb.edu.au

Notes. The authors declare no competing financial interest.

Acknowledgements

This research was supported by the Australian Research Council (ARC) under the Australian Laureate Fellowship scheme (FL120100030), and by the ARC Centre of Excellence in Convergent Bio-Nano Science and Technology (Project No. CE140100036). This work was performed in part at the Materials Characterisation and Fabrication Platform at the University of Melbourne and the Victorian Node of the Australian National Fabrication Facility.

References

1. Ejima, H.; Richardson, J. J.; Liang, K.; Best, J. P.; van Koeverden, M. P.; Such, G. K.; Cui, J.; Caruso, F., One-Step Assembly of Coordination Complexes for Versatile Film and Particle Engineering. *Science* **2013,** *341*, 154-157.
2. Guo, J.; Ping, Y.; Ejima, H.; Alt, K.; Meissner, M.; Richardson, J. J.; Yan, Y.; Peter, K.; von Elverfeldt, D.; Hagemeyer, C. E.; Caruso, F., Engineering Multifunctional Capsules through the Assembly of Metal–Phenolic Networks. *Angew. Chem., Int. Ed.* **2014,** *53*, 5546-5551.

3. Yang, L.; Han, L.; Ren, J.; Wei, H.; Jia, L., Coating Process and Stability of Metal-Polyphenol Film. *Colloids Surf., A* **2015,** *484*, 197-205.
4. Ejima, H.; Richardson, J. J.; Caruso, F., Metal-Phenolic Networks as a Versatile Platform to Engineer Nanomaterials and Biointerfaces. *Nano Today* **2017,** *12*, 136-148.
5. Björnmalm, M.; Cui, J.; Bertleff-Zieschang, N.; Song, D.; Faria, M.; Rahim, M. A.; Caruso, F., Nanoengineering Particles through Template Assembly. *Chem. Mater.* **2016,** *29*, 289–306.
6. Rahim, M. A.; Kempe, K.; Müllner, M.; Ejima, H.; Ju, Y.; van Koeverden, M. P.; Suma, T.; Braunger, J. A.; Leeming, M. G.; Abrahams, B. F.; Caruso, F., Surface-Confined Amorphous Films from Metal-Coordinated Simple Phenolic Ligands. *Chem. Mater.* **2015,** *27*, 5825-5832.
7. Bertleff-Zieschang, N.; Rahim, M. A.; Ju, Y.; Braunger, J. A.; Suma, T.; Dai, Y.; Pan, S.; Cavalieri, F.; Caruso, F., Biofunctional Metal-Phenolic Films from Dietary Flavonoids. *Chem. Commun.* **2017,** *53*, 1068-1071.
8. Ball, V., Electrodeposition of Pyrocatechol Based Films: Influence of Potential Scan Rate, Pyrocatechol Concentration and pH. *Colloids Surf., A* **2017,** *518*, 109-115.
9. Rahim, M. A.; Björnmalm, M.; Suma, T.; Faria, M.; Ju, Y.; Kempe, K.; Müllner, M.; Ejima, H.; Stickland, A. D.; Caruso, F., Metal–Phenolic Supramolecular Gelation. *Angew. Chem., Int. Ed.* **2016,** *55*, 13803-13807.
10. Lee, H.; Dellatore, S. M.; Miller, W. M.; Messersmith, P. B., Mussel-Inspired Surface Chemistry for Multifunctional Coatings. *Science* **2007,** *318*, 426-430.
11. Lee, M.; Rho, J.; Lee, D.-E.; Hong, S.; Choi, S.-J.; Messersmith, P. B.; Lee, H., Water Detoxification by a Substrate-Bound Catecholamine Adsorbent. *ChemPlusChem* **2012,** *77*, 987-990.
12. Ku, S. H.; Ryu, J.; Hong, S. K.; Lee, H.; Park, C. B., General Functionalization Route for Cell Adhesion on Non-Wetting Surfaces. *Biomaterials* **2010,** *31*, 2535-2541.
13. Park, H.-J.; Yang, K.; Kim, M.-J.; Jang, J.; Lee, M.; Kim, D.-W.; Lee, H.; Cho, S.-W., Bio-Inspired Oligovitronectin-Grafted Surface for Enhanced Self-Renewal and Long-Term Maintenance of Human Pluripotent Stem Cells under Feeder-Free Conditions. *Biomaterials* **2015,** *50*, 127-139.
14. Wang, J.-G.; Hua, X.; Li, M.; Long, Y.-T., Mussel-Inspired Polydopamine Functionalized Plasmonic Nanocomposites for Single-Particle Catalysis. *ACS Appl. Mater. Interfaces* **2017,** *9*, 3016-3023.

15. Postma, A.; Yan, Y.; Wang, Y.; Zelikin, A. N.; Tjipto, E.; Caruso, F., Self-Polymerization of Dopamine as a Versatile and Robust Technique to Prepare Polymer Capsules. *Chem. Mater.* **2009,** *21*, 3042-3044.
16. Liu, Y.; Ai, K.; Lu, L., Polydopamine and Its Derivative Materials: Synthesis and Promising Applications in Energy, Environmental, and Biomedical Fields. *Chem. Rev.* **2014,** *114*, 5057-5115.
17. Liu, X.; Cao, J.; Li, H.; Li, J.; Jin, Q.; Ren, K.; Ji, J., Mussel-Inspired Polydopamine: A Biocompatible and Ultrastable Coating for Nanoparticles in Vivo. *ACS Nano* **2013,** *7*, 9384-9395.
18. Rahim, M. A.; Björnmalm, M.; Bertleff-Zieschang, N.; Besford, Q.; Mettu, S.; Suma, T.; Faria, M.; Caruso, F., Rust-Mediated Continuous Assembly of Metal–Phenolic Networks. *Adv. Mater.* **2017,** *29*, 1606717.
19. Han, P.; Shi, J.; Nie, T.; Zhang, S.; Wang, X.; Yang, P.; Wu, H.; Jiang, Z., Conferring Natural-Derived Porous Microspheres with Surface Multifunctionality through Facile Coordination-Enabled Self-Assembly Process. *ACS Appl. Mater. Interfaces* **2016,** *8*, 8076-8085.
20. Liang, H.; Li, J.; He, Y.; Xu, W.; Liu, S.; Li, Y.; Chen, Y.; Li, B., Engineering Multifunctional Films Based on Metal-Phenolic Networks for Rational pH-Responsive Delivery and Cell Imaging. *ACS Biomater. Sci. Eng.* **2016,** *2*, 317-325.
21. Ju, Y.; Dai, Q.; Cui, J.; Dai, Y.; Suma, T.; Richardson, J. J.; Caruso, F., Improving Targeting of Metal–Phenolic Capsules by the Presence of Protein Coronas. *ACS Appl. Mater. Interfaces* **2016,** *8*, 22914-22922.
22. Ozawa, H.; Haga, M.-A., Soft Nano-Wrapping on Graphene Oxide by Using Metal-Organic Network Films Composed of Tannic Acid and Fe Ions. *Phys. Chem. Chem. Phys.* **2015,** *17*, 8609-8613.
23. Bray, K.; Previdi, R.; Gibson, B. C.; Shimoni, O.; Aharonovich, I., Enhanced Photoluminescence from Single Nitrogen-Vacancy Defects in Nanodiamonds Coated with Phenol-Ionic Complexes. *Nanoscale* **2015,** *7*, 4869-4874.
24. Çakar, S.; Güy, N.; Özacar, M.; Fındık, F., Investigation of Vegetable Tannins and Their Iron Complex Dyes for Dye Sensitized Solar Cell Applications. *Electrochim. Acta* **2016,** *209*, 407-422.
25. Shen, G.; Xing, R.; Zhang, N.; Chen, C.; Ma, G.; Yan, X., Interfacial Cohesion and Assembly of Bioadhesive Molecules for Design of Long-Term Stable Hydrophobic Nanodrugs toward Effective Anticancer Therapy. *ACS Nano* **2016,** *10*, 5720-5729.

26. Song, Y.-Z.; Kong, X.; Yin, X.; Zhang, Y.; Sun, C.-C.; Yuan, J.-J.; Zhu, B.; Zhu, L.-P., Tannin-Inspired Superhydrophilic and Underwater Superoleophobic Polypropylene Membrane for Effective Oil/Water Emulsions Separation. *Colloids Surf., A* **2017,** *522*, 585-592.
27. Liang, H.; Zhou, B.; Li, J.; Pei, Y.; Li, B., Coordination-Driven Multilayer of Phosvitin-Polyphenol Functional Nanofibrous Membranes: Antioxidant and Biomineralization Applications for Tissue Engineering. *RSC Adv.* **2016,** *6*, 98935-98944.
28. Balasundram, N.; Sundram, K.; Samman, S., Phenolic Compounds in Plants and Agri-Industrial By-Products: Antioxidant Activity, Cccurrence, and Potential Uses. *Food Chem.* **2006,** *99*, 191-203.
29. Manach, C.; Scalbert, A.; Morand, C.; Rémésy, C.; Jiménez, L., Polyphenols: Food Sources and Bioavailability. *Am. J. Clin. Nutr.* **2004,** *79*, 727-747.
30. Kähkönen, M. P.; Hopia, A. I.; Vuorela, H. J.; Rauha, J.-P.; Pihlaja, K.; Kujala, T. S.; Heinonen, M., Antioxidant Activity of Plant Extracts Containing Phenolic Compounds. *J. Agric. Food. Chem.* **1999,** *47*, 3954-3962.
31. Raymond, K. N.; Allred, B. E.; Sia, A. K., Coordination Chemistry of Microbial Iron Transport. *Acc. Chem. Res.* **2015,** *48*, 2496-2505.
32. Krogsgaard, M.; Nue, V.; Birkedal, H., Mussel-Inspired Materials: Self-Healing through Coordination Chemistry. *Chem. Eur. J.* **2016,** *22*, 844-857.
33. Ma, S.; Lee, H.; Liang, Y.; Zhou, F., Astringent Mouthfeel as a Consequence of Lubrication Failure. *Angew. Chem., Int. Ed.* **2016,** *55*, 5793-5797.
34. Hodgson, J. M.; Croft, K. D., Tea Flavonoids and Cardiovascular Health. *Mol. Aspects Med.* **2010,** *31*, 495-502.
35. Graham, H. N., Green Tea Composition, Consumption, and Polyphenol Chemistry. *Prev. Med.* **1992,** *21*, 334-350.
36. Thielecke, F.; Boschmann, M., The Potential Role of Green Tea Catechins in the Prevention of the Metabolic Syndrome – A Review. *Phytochemistry* **2009,** *70*, 11-24.
37. Botten, D.; Fugallo, G.; Fraternali, F.; Molteni, C., Structural Properties of Green Tea Catechins. *J. Phys. Chem. B* **2015,** *119*, 12860-12867.
38. Singh, B. N.; Shankar, S.; Srivastava, R. K., Green Tea Catechin, Epigallocatechin-3-Gallate (EGCG): Mechanisms, Perspectives and Clinical Applications. *Biochem. Pharmacol.* **2011,** *82*, 1807-1821.

39. Lee, H.; Shim, W.; Kim, C. E.; Choi, S. Y.; Lee, H.; Yang, J., Therapeutic Efficacy of Nanocomplex of Poly(Ethylene Glycol) and Catechin for Dry Eye Disease in a Mouse Model. *Invest. Ophthalmol. Vis. Sci.* **2017,** *58*, 1682-1691.
40. Kharissova, O. V.; Dias, H. V. R.; Kharisov, B. I.; Pérez, B. O.; Pérez, V. M. J., The Greener Synthesis of Nanoparticles. *Trends Biotechnol.* **2013,** *31*, 240-248.
41. Ahmed, S.; Ahmad, M.; Swami, B. L.; Ikram, S., A Review on Plants Extract Mediated Synthesis of Silver Nanoparticles for Antimicrobial Applications: A Green Expertise. *J. Adv. Res.* **2016,** *7*, 17-28.
42. Xiao, L.; Mertens, M.; Wortmann, L.; Kremer, S.; Valldor, M.; Lammers, T.; Kiessling, F.; Mathur, S., Enhanced In Vitro and In Vivo Cellular Imaging with Green Tea Coated Water-Soluble Iron Oxide Nanocrystals. *ACS Appl. Mater. Interfaces* **2015,** *7*, 6530-6540.
43. Sileika, T. S.; Barrett, D. G.; Zhang, R.; Lau, K. H. A.; Messersmith, P. B., Colorless Multifunctional Coatings Inspired by Polyphenols Found in Tea, Chocolate, and Wine. *Angew. Chem., Int. Ed.* **2013,** *52*, 10766-10770.
44. Shishikura, Y.; Khokhar, S., Factors Affecting the Levels of Catechins and Caffeine in Tea Beverage: Estimated Daily Intakes and Antioxidant Activity. *J. Sci. Food Agric.* **2005,** *85*, 2125-2133.
45. Saklar, S.; Ertas, E.; Ozdemir, I. S.; Karadeniz, B., Effects of Different Brewing Conditions on Catechin Content and Sensory Acceptance in Turkish Green Tea Infusions. *J. Food Sci. Technol.* **2015,** *52*, 6639-6646.
46. Rahim, M. A.; Ejima, H.; Cho, K. L.; Kempe, K.; Müllner, M.; Best, J. P.; Caruso, F., Coordination-Driven Multistep Assembly of Metal–Polyphenol Films and Capsules. *Chem. Mater.* **2014,** *26*, 1645-1653.
47. Wang, K.; Ruan, J., Analysis of Chemical Components in Green Tea in Relation with Perceived Quality, a Case Study with Longjing Teas. *Int. J. Food Sci. Technol.* **2009,** *44*, 2476-2484.
48. Ramdani, D.; Chaudhry, A. S.; Seal, C. J., Chemical Composition, Plant Secondary Metabolites, and Minerals of Green and Black Teas and the Effect of Different Tea-to-Water Ratios during Their Extraction on the Composition of Their Spent Leaves as Potential Additives for Ruminants. *J. Agric. Food. Chem.* **2013,** *61*, 4961-4967.
49. Granato, D.; Prado-Silva, L. d.; Alvarenga, V. O.; Zielinski, A. A. F.; Bataglion, G. A.; Morais, D. R. d.; Eberlin, M. N.; Sant'Ana, A. d. S., Characterization of Binary and Ternary Mixtures of Green, White and Black Tea Extracts by Electrospray Ionization

Mass Spectrometry and Modeling of Their In Vitro Antibacterial Activity. *LWT-Food Sci. Technol.* **2016,** *65*, 414-420.

50. Balentine, D. A.; Wiseman, S. A.; Bouwens, L. C. M., The Chemistry of Tea Flavonoids. *Crit. Rev. Food Sci. Nutr.* **1997,** *37*, 693-704.
51. Manning, J.; Roberts, J. C., Analysis of Catechin Content of Commercial Green Tea Products. *J. Herb. Pharmacother.* **2003,** *3*, 19-32.
52. Tao, W.; Zhou, Z.; Zhao, B.; Wei, T., Simultaneous Determination of Eight Catechins and Four Theaflavins in Green, Black and Oolong Tea Using new HPLC–MS–MS Method. *J. Pharm. Biomed. Anal.* **2016,** *131*, 140-145.
53. Sever, M. J.; Wilker, J. J., Visible Absorption Spectra of Metal-Catecholate and Metal-Tironate Complexes. *Dalton Trans.* **2004**, 1061-1072.
54. Perron, N. R.; Wang, H. C.; DeGuire, S. N.; Jenkins, M.; Lawson, M.; Brumaghim, J. L., Kinetics of Iron Oxidation Upon Polyphenol Binding. *Dalton Trans.* **2010,** *39*, 9982-9987.
55. Li, Q.; Barrett, D. G.; Messersmith, P. B.; Holten-Andersen, N., Controlling Hydrogel Mechanics via Bio-Inspired Polymer–Nanoparticle Bond Dynamics. *ACS Nano* **2016,** *10*, 1317-1324.
56. Holten-Andersen, N.; Harrington, M. J.; Birkedal, H.; Lee, B. P.; Messersmith, P. B.; Lee, K. Y. C.; Waite, J. H., pH-Induced Metal-Ligand Cross-Links Inspired by Mussel Yield Self-Healing Polymer Networks with Near-Covalent Elastic Moduli. *Proc. Natl. Acad. Sci. U. S. A.* **2011,** *108*, 2651-2655.
57. Berry, J. D.; Mettu, S.; Dagastine, R. R., Precise Measurements of Capsule Mechanical Properties using Indentation. *Soft Matter* **2017,** *13*, 1943-1947.

Table of Content graphic